Non-linear response of PM2.5 to changes in NO$_x$ and NH$_3$ emissions in the Po basin (Italy): consequences for air quality plans

Philippe Thunis[1], Alain Clappier[2], Matthias Beekmann[3], Jean Philippe Putaud[1], Cornelis
5   Cuvelier[4], Jessie Madrazo[5], Alexander de Meij[6]

[1] European Commission, Joint Research Centre, Ispra, Italy

[2] Université de Strasbourg, Laboratoire Image Ville Environnement, Strasbourg, France

[3] Laboratoire Interuniversitaire des Systèmes Atmosphériques, UMR CNRS 7583, Université Paris Est Créteil et
10   Université de Paris, Institut Pierre Simon Laplace, Créteil, France

[4] Ex European Commission, Joint Research Centre, Ispra, Italy

[5] Signa Terre SA, Geneva, Switzerland

[6] MetClim, Varese, Italy

15   Corresponding author: Philippe Thunis (philippe.thunis@ec.europea,eu)

Abstract: Air pollution is one of the main causes of damages to human health in Europe with an estimate of about
380 000 premature deaths per year in the EU28, as the result of exposure to fine particulate matter (PM2.5) only. In
this work, we focus on one specific region in Europe, the Po basin, a region where chemical regimes are the most
20   complex, showing important non-linear processes, especially those related to interactions between NO$_x$ and NH$_3$. We
analyse the sensitivities of PM2.5 to NO$_x$ and NH$_3$ emissions by means of a set of EMEP simulations performed with
different levels of emission reductions, from 25% up to a total switch-off of those emissions. Both single and combined
precursor reduction scenarios are applied to determine the most efficient emission reduction strategies and quantify
the interactions between NO$_x$ and NH$_3$ emission reductions. The results confirmed the peculiarity of secondary PM2.5
25   formation in the Po basin, characterised by contrasting chemical regimes within distances of few (hundreds of)
kilometres, as well as strong non-linear responses to emission reductions during wintertime. One of the striking results
is the increase of the PM2.5 concentration levels when NO$_x$ emission reductions are applied in NO$_x$-rich areas, such
as the surroundings of Bergamo. The increased oxidative capacity of the atmosphere is the cause of the increase of
PM2.5 induced by a reduction in NO$_x$ emission. This process can have contributed to the absence of significant PM2.5
30   concentration decrease during the COVID-19 lockdowns in many European cities. It is important to account for this
process when designing air quality plans, since it could well lead to transitory increases in PM2.5 at some locations
in winter as NO$_x$ emission reduction measures are gradually implemented. While PM2.5 responses to NO$_x$ and NH$_3$
emission reduction show large variations seasonally and spatially, these responses remain close to linear, i.e.
proportional to the emission reduction levels, at least up to -50% because secondary aerosol formation chemical
35   regimes are not modified by those relatively moderate ranges.

Keywords: urban air pollution, air quality planning, non-linearity, chemical regimes

1. Introduction

40   Air pollution is one of the main causes of damages to human health in Europe with an estimate of about 380 000
premature deaths per year in the EU28, as the result of exposure to fine particulate matter (PM2.5) only (EEA,
2020). Many of the exceedances to the EU limit values occur in urban areas where most of the population is
exposed.

PM2.5 is partly emitted directly (primary particles) and partly formed through photo-chemical reactions that involve gaseous precursors like SO_x, NO_x, NH_3 and non-methane volatile organic compounds (NMVOC) to form secondary inorganic and organic aerosol (SIA and SOA). The secondary fraction is often dominating the total concentration of particulate matter in urban areas as shown by e.g., Beekmann et al. (2015) for the Greater Paris region, De Meij et al. (2006, 2009) or Larsen et al. (2012) in northern Italy, hence the importance to understand the complex chemical processes that lead to its formation. In particular, it is key to identify the precursors involved in these reactions in order to target the right sectors of activity in air quality plans to effectively reduce pollution levels. According to the EDGAR estimates for 2015 (EDGAR, 2020) for Italy, about 90% of the NH_3 is directly emitted in the atmosphere by the agriculture sector while SO_x precursors are predominantly released by the energy production and use (industrial) sectors, about 90% (EDGAR estimates for 2015). For NO_x, emissions are spread among various sectors, with transport (50%), industry (40%) and agriculture (4%) being the main ones. The gaseous precursors of secondary organic aerosols (SOA) include a vast range of high- and low-volatility NMVOCs among which biogenic terpenes and anthropogenic aromatics. The main sources of aromatics in Italy were in 2012 transport (58%), use of fuels and solvents (32%), and domestic heating (15%).

Regarding SIA, early works used box models with thermodynamic schemes to address the sensitivity of ammonium nitrate and sulfate concentrations to gaseous NH_3, NO_x, and SO_2 emissions (Watson et al., 1994; Blanchard and Hidy, 2003). These models were later on integrated into chemical transport models (CTM), in particular to address the benefit of additional NH_3 emissions reductions in addition to already ongoing SO_2 and NO_x emission reductions. For North America, Makar et al. (2009) simulated with a regional CTM that a 30% reduction of ammonia emissions would lead to about 1 µg/m³ reduction in PM2.5. For Europe, Bessagnet et al. (2014) simulated the effects of a 30% NH_3 emission reduction in addition to those foreseen by the Gothenburg Protocol for 2030, and found that the G-ratio defined as the ratio between free ammonia and total nitrate (Ansari and Pandis, 1998) was a good predictor for the efficiency of NH_3 reductions on SIA concentrations. These sensitivities to emission reductions are often governed by complex chemical mechanisms. A well described phenomenon is the release of free ammonia as a result of decreased SO_2 emissions and sulfate formation, which allows for the formation of additional nitrate, for example Blanchard and Hidy (2003) and Shah et al. (2018) for wintertime PM2.5 over the Eastern US. For eastern China, Fu et al. (2017) and Lachatre et al. (2019) showed both from modelling and satellite observations that this processes leads to strongly increased ammonia tropospheric columns. Finally, several works compared CTM simulations to specific observations. For instance, Pay et al. (2012) showed that the G –ratio was generally underestimated over Europe, inducing that the Caliope model they used could probably overestimate the efficiency of NH_3 emission reductions. Petetin et al. (2016) came to a similar conclusion comparing CHIMERE CTM simulations to observations in the Paris region. They ascribed this underestimation to missing NH_3 emissions especially during warmer periods.

The formation of SOA results from even more complex reactions involving photo-chemical oxidation (as for SIA), nitration, fragmentation, and oligomerisation of gaseous precursors or secondary products (Kroll and Seinfeld, 2008; Shrivastava et al., 2017). Models generally use simplified parameterizations to calculate the SOA formation yield from various classes of parent VOCs (Tsigaridis et al., 2014), and comparison with measurements often show that SOA sources are still missing in models (Huang et al., 2020).

In this work, we focus on one specific region in Europe, the Po basin. In a companion paper (Clappier et al., 2020) that analyses PM secondary formation chemical regimes across Europe, the Po basin is clearly identified as a peculiar area where the chemical regime distributions are the most complex, showing important non-linear processes (Thunis et al., 2013 and 2015; Carnevale, 2020; Bessagnet, 2014), especially those related to interactions between NO_x and NH_3. The Po basin is also one of the pollution hot spots in Europe where the number of days above the limit values prescribed by the AAQD for PM10 is yet largely exceeded (EEA, 2020). This situation results from the high emission density in this region and also from the geographical setting of the area, in border of the Alps and Apennines mountain ranges that lead to very weak winds in the area, favouring the accumulation of atmospheric pollutants.

We focus the present analysis on the NH_3-NO_x chemical processes and describe their spatial and seasonal variability, which could help to design more effective mitigation strategies. We start by describing the modelling set-up and detail the series of simulations required to perform our analysis. Section 3 provides a brief overview of the modelled base-case concentrations. In Section 4, we analyse the sensitivity of PM2.5 concentrations to NH_3 and

95   NO$_x$ emissions. Section 5 provides an analysis of the non-linearity in PM2.5 response to these emissions while in
Section 6, we discuss the implications of these results in terms of mitigation measures and design of air quality
plans. Conclusions are finally proposed.

2.   Methodology

2.1   Modelling set-up

100   The modelling study is performed with the EMEP/MSC-W air quality model, version rv4_17 (Simpson et al., 2012).
The emission input consists of gridded annual national emissions (SO$_2$, NO, NO$_2$, NH$_3$, NMVOC, CO and primary
PM2.5) at 0.1×0.1 degrees resolution, based on data reported every year by parties to the Convention on Long
Range Transboundary Air Pollution (CLRTAP). These emissions are provided for 10 anthropogenic source-sectors
classified by SNAP (Selected Nomenclature for Air Pollution) codes (EMEP, 2003). Meteorological input data are
105   based on forecasts from the Integrated Forecast System (IFS), a global operational forecasting model from the
European Centre for Medium-Range Weather Forecasts (ECMWF). Meteorological fields are retrieved at a 0.1×0.1
degree longitude latitude resolution and are interpolated to the 50×50km^2 polar-stereographic grid projection
(EMEP, 2011).

The modelling domain covers the entire Po basin (Figure 1) with a resolution of 0.1 by 0.1-degree resolution (polar
110   stereographic projection centred at 60 °N) and includes 20 vertical levels. The initial and background concentrations
for ozone are based on Logan (1998) climatology, as described in Simpson et al. (2003). For the other species,
background/initial conditions are set within the model using functions based on observations (Simpson et al., 2003
and Fagerli et al., 2004). The simulations cover the entire meteorological year 2015. We will not discuss the
validation of the base-case simulation, as this is available in other publications (e.g. Simpson et al., 2012) and
115   regular status reports by EMEP (https://emep.int/mscw/mscw_publications.html).

In this work, we simulated a series of 24 scenarios in which NO$_x$ and NH$_3$ emissions were reduced independently or
simultaneously by 25, 50, 75 and 100% from the base case reference levels. Emission reductions were applied over
the entire Po-basin domain for a complete meteorological year (2015).

2.2   Spatial and temporal focus

120   Results are generally presented in terms of maps but three locations within the domain were selected for a more
detailed analysis. The locations are Bergamo (Be) in the northern part of the domain, Mantova (Ma) in the central
eastern part of the Po basin and Bologna (Bo) in its southern part. As described in the following sections, we will
see that these locations show very different behaviours in terms of response to emission changes.

We also aggregate results into 2 seasons: winter and summer that cover the period from November to February and
125   from April to September, respectively. These two seasons are characteristic of different chemical regimes as
illustrated in the following sections. The process to define the temporal bounds of these two seasons is discussed in
Annex 1. The two remaining months (March and October) represent transition periods and are not considered in our
analysis.

As we only analyse the processes involving inorganic gas-phase precursors, our focus is on secondary inorganic
130   PM2.5 although most of the results are expressed in terms of total PM2.5 concentrations. The impact of NO$_x$
emission reductions on SOA concentration is only briefly discussed in section 5.

2.3   Indicators

To describe the interactions between NH$_3$ and NO$_x$ emissions, we use the relationship proposed by Stein and Alpert
(1993) and Thunis and Clappier (2014). This relation expresses the change of concentration resulting from a
135   reduction of both precursors NO$_x$ and NH$_3$ simultaneously, as the sum of two single concentration changes and an
interaction term, as follows:

$$\Delta C_{NO_xNH_3}^{\alpha} = \Delta C_{NO_x}^{\alpha} + \Delta C_{NH_3}^{\alpha} + \hat{C}_{NO_xNH_3}^{\alpha} \tag{1}$$

Where ΔC stands for the PM2.5 concentration change (reference minus scenario) for a percentage α emission reduction (thus the term $\Delta C/\alpha$ is defined positive for a concentration reduction, consecutive to an emission reduction) and $\hat{C}$ for the interaction term. We then scale each of these terms by the emission reduction (α) to generate potentials (P) (Thunis and Clappier, 2014).

$$\frac{\Delta C^{\alpha}_{NO_xNH_3}}{\alpha} = P^{\alpha}_{NO_xNH_3} = P^{\alpha}_{NO_x} + P^{\alpha}_{NH_3} + \hat{P}^{\alpha}_{NO_xNH_3} = \frac{\Delta C^{\alpha}_{NO_x}}{\alpha} + \frac{\Delta C^{\alpha}_{NH_3}}{\alpha} + \frac{\hat{C}^{\alpha}_{NO_xNH_3}}{\alpha} \qquad (2)$$

This division by the factor α is a mean to virtually extrapolate the impact resulting from any percentage emission reduction from 1 to 100%. Potentials facilitate the comparison of concentration changes obtained for different emission reduction levels. Indeed, equal potentials imply a linear relationship between emission reductions and concentration changes. For example, $P^{\alpha} = P^{\beta} \Rightarrow \Delta C^{\alpha} = \frac{\alpha}{\beta}\Delta C^{\beta}$, for α and β, two emission reduction levels.

The overall potential is therefore the sum of two single potentials and one interaction term.

A relation between the potentials of combined emission reductions at two levels of intensity, is obtained by writing (2) for two reduction levels α and β and subtract the two equations. This leads to the following relation:

$$P^{\beta}_{NO_xNH_3} = P^{\alpha}_{NO_xNH_3} + \underbrace{P^{\beta}_{NO_x} - P^{\alpha}_{NO_x}}_{P^{\beta-\alpha}_{NOx}} + \underbrace{P^{\beta}_{NH_3} - P^{\alpha}_{NH_3}}_{P^{\beta-\alpha}_{NH_3}} + \underbrace{\hat{P}^{\beta}_{NO_xNH_3} - \hat{P}^{\alpha}_{NO_xNH_3}}_{\hat{P}^{\beta-\alpha}_{NOxNH_3}} \qquad (3)$$

or equivalently via equation 2:

$$P^{\beta}_{NO_xNH_3} = P^{\alpha}_{NO_x} + P^{\alpha}_{NH_3} + \underbrace{\hat{P}^{\alpha}_{NO_xNH_3} + \hat{P}^{\beta-\alpha}_{NOx} + \hat{P}^{\beta-\alpha}_{NH3} + \hat{P}^{\beta-\alpha}_{NOxNH3}}_{non-linear\ terms} \qquad (4)$$

While the two first terms on the right hand side of Eq. 4 represent the single potentials, the remaining right hand side terms quantify the magnitude of non-linearities. $\hat{P}^{\alpha}_{NO_xNH_3}$ quantifies the NO$_x$-NH$_3$ interaction at level α, $\hat{P}^{\beta-\alpha}_{NOx}$ and $\hat{P}^{\beta-\alpha}_{NH3}$ are the single non-linearities associated to NO$_x$ and NH$_3$ emissions, respectively, between levels α and β, whereas $\hat{P}^{\beta-\alpha}_{NOxNH3}$ represents the incremental change of the NO$_x$-NH$_3$ interaction between levels α and β.

Information about non-linearity is important to design air quality plans as it informs on the robustness of a given response, i.e. whether or not this response remains valid over a certain range and type of emission reductions. Because air quality models often provide responses for a limited set of scenarios that are then used as a basis to interpolate/extrapolate the responses to other emission reduction levels, robustness shall always be carefully assessed.

In the next section, we present the baseline results in terms of spatial and temporal variations.

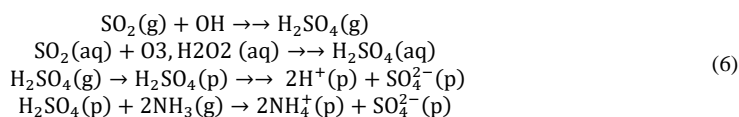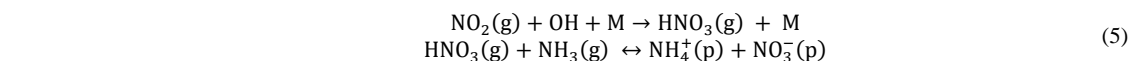### 3. Baseline concentrations of PM2.5 and gaseous inorganic precursors

Before analysing the impact of emission changes on concentrations, it is worth having a look at the baseline concentration fields. In Figure 1, the yearly averaged PM2.5 concentration fields show a widespread pollution plume covering most of the area, with peak values extending in its central part. The maximum modelled yearly values reach 29 $\mu g/m^3$, that represent an average between maximum winter values (maximum of 59 $\mu g/m^3$) and minimum summer values (17 $\mu g/m^3$).

The seasonal fields of PM2.5 clearly show that high yearly average values mostly result from the winter season contributions when more stable atmospheric conditions lead to stagnant conditions, favouring the accumulation of particulate matter in the area (Pernigotti et al., 2014; Raffaelli et al., 2020). The increased emissions from the

Atmospheric
Chemistry
and Physics
Discussions

residential sector (heating, especially wood burning) also foster this process (Ricciardelli et al., 2017; Hakimzadeh et al., 2020). The relative contribution of secondary inorganic particles (SIA) ranges between 40 and 50%,
175 regardless of the season and is quite homogeneously distributed spatially over the entire area. Strategies targeting SIA have therefore the potential to abate about half of the total PM2.5 concentration.

As mentioned earlier, the secondary inorganic fraction of PM2.5 results from complex atmospheric processes that involve gaseous precursors (mainly SO_2, NO_x and NH_3), that can be summarized by the two following chemical pathways:

$$NO_2(g) + OH + M \rightarrow HNO_3(g) \ + \ M$$
$$HNO_3(g) + NH_3(g) \ \leftrightarrow NH_4^+(p) + NO_3^-(p)$$

(5)

180

$$SO_2(g) + OH \rightarrow\rightarrow H_2SO_4(g)$$
$$SO_2(aq) + O3, H2O2 \ (aq) \rightarrow\rightarrow H_2SO_4(aq)$$
$$H_2SO_4(g) \rightarrow H_2SO_4(p) \rightarrow\rightarrow \ 2H^+(p) + SO_4^{2-}(p)$$
$$H_2SO_4(p) + 2NH_3(g) \rightarrow 2NH_4^+(p) + SO_4^{2-}(p)$$

(6)

where (g) means "gas phase", (aq) aqueous phase, while (p) means "particulate matter", and the character $\rightarrow\rightarrow$ symbolizes a chemical pathway that summarizes a set of underlying reactions.

The second of these pathways is generally slower than the first one, the NO_2 oxidation specific time constant being
185 typically some hours to a day, and that of SO_2 one to several days (Seinfeld and Pandis, 2006).

The spatial fields for the seasonal average concentrations of these precursors (Figure 2) reflects their emissions spatial patterns resulting in a NO_2-rich area that comprises Milan plus its northern districts (and to a lesser extent, Turin), while NH_3 is more abundant in the central part of the Po basin, east of Milan, where intensive agriculture
190 practices take place. Finally, high SO_2 concentrations are collocated with the NO_2-rich areas nearby Milan but with an additional zone around the harbour city of Genova (along the south coast), reflecting the more important SO_2 emissions from the shipping sector there. However, SO_2 concentrations are about one order of magnitude below those of NO_2. Seasonal variations are well marked for NO_2 and SO_2 concentrations, not so much in terms of minimum and maximum values but rather in terms of spread with an extended high concentration zone covered
195 during wintertime. In contrast, NH_3 concentrations remain very similar in summer and winter, both in terms of values and spatial distribution.

In next sections, we simulate a series of emission reduction scenarios to analyse the response of PM2.5 concentration to single and combined reductions of NH_3 and NO_x.

4. Analysis of the SIA formation chemical regimes

200 ### 4.1 Seasonal trends
From a strategic point of view, it is important to know whether NO_x (mostly emitted by the transport, industry and residential sectors) or NH_3 (mostly emitted by agriculture) need to be reduced in priority in order to reach effective results on particulate pollution mitigation. In Clappier et al. (2020), we have observed a great heterogeneity in SIA formation chemical regimes across the Po-basin, different regimes being present in limited geographical areas. Here
205 we intend to look at these regimes in more detail.

To analyse in details the chemical regimes in the Po basin, we compare the two single potentials $P_{NO_x}^{25\%}, P_{NH_3}^{25\%}$ obtained for moderate emission reduction of 25% (). Figure 3 provides a spatial overview of the difference between these two potentials ($P_{NO_x}^{25\%} - P_{NH_3}^{25\%}$). This indicator tells whether reductions of NO_x of NH_3 will lead to the greatest PM2.5 concentration abatement, i.e. if the regime is rather NO_x- or NH_3-sensitive, with positive and negative values,
210 respectively.

- During summer time (Figure 3 – left), the entire area is under weak NO_x-sensitive conditions with a maximum intensity in its central part, between Bergamo and Mantova.
- During wintertime (Figure 3 – right), the situation is contrasted with a wide and intense NH_3-sensitive area that appears around and south-eastwards of Bergamo. This area includes big cities like Milan. Other (not as marked) NH_3 sensitive regime zones appear nearby coastal areas. Most strongly NO_x-sensitive areas are located in the eastern parts of the domain, north of Bologna and Venice. As expected, NH_3-sensitive regimes are collocated with the NO_2- and SO_2- rich areas (Figure 2), whereas NO_x-sensitive regimes coincide with NH_3-rich areas. The cases of the three selected cities (Bergamo, Mantova and Bologna) representative of the NH_3-sensitive, NO_x-sensitive and neutral regimes, respectively, are further analysed below. The chemical regimes deducted from the results of emission reduction scenarios can be compared with the maps of the G-ratio (Figure 4), defined by Ansari and Pandis (1998) as the ratio between free ammonia (NH_3 and NH_4^+) and total nitrate ($HNO_3 + NO_3^-$) after neutralization of H_2SO_4. Values of the G-ratio below 1 indicate a NH_3-limited chemical regime, while values above 1 characterize a HNO_3-limited chemical regime.

$$G = \frac{NH_3(g) + NH_4^+(p) - 2SO_4^{2-}(p)}{HNO_3(g) + NO_3^-(p)} \tag{7}$$

We first note that that formulation of the G-ratio, in terms of abundance of free total ammonia and total nitrate, differs from that of the NH_3 and NOx emission sensitive chemical regime. The following discussion tends to show how both diagnostics can be used in a complementary way. During summer, the G-ratio values well above unity indicate a HNO_3 limited chemical regime across the Po basin. This corresponds to a NOx sensitive chemical regime in this region. Moreover, the location of the G-ratio maximum between Bergamo and Modena spatially coincides with the most pronounced NO_x sensitive regime, and to a maximum of NH_3 concentrations of about 20 µg/m^3 (Figure 2). Indeed, NO_x emission reductions lead to HNO_3 concentration reductions that is the limiting factor in NH_4NO_3 formation according to the G-ratio. During winter, the G-ratio still shows large values in the region south-east of Bergamo, but contrary to winter, the chemical regime is clearly NH_3 sensitive. More generally, G-ratio values remain above unity over the whole Po basin while both NO_x and NH_3 sensitive chemical regimes prevail in different areas. Thus, even if free total ammonia is more abundant, PM abatement is more sensitive to NH_3 than to NO_x emissions. These differences illustrate the impossibility to directly use the G-ratio for air quality management, an interesting result in itself. We will further discuss this interesting behaviour later when addressing non-linearity in section 4.3.

4.2 Impact of the emission reduction strength

In this section, we repeat the analysis of Section 4.1 for yearly average concentrations but looking at the step changes of regimes as we progressively remove emissions from the base case situation. (Figure 5). Chemical regimes are well in place for a 25% level reduction (top left) and are only slightly perturbed from 25 to 50% with a reinforcement of the NOx limited regime (top right). . Despite this slight change in intensity, the regimes keep therefore the same spatial patterns. From 50% onward, chemical regimes tend to attenuate and reverse themselves from 75% to 100% (bottom right).

In other words, locations that are NH_3-sensitive for moderate reductions become NO_x-sensitive for larger reductions, and vice versa.

4.3 A summarized overview: the PM2.5 isopleths

Like isopleth plots that show the variations in the O_3 concentrations as a function of NO_x and VOC concentrations (Dodge, 1977), similar plots can be created for PM2.5 concentrations as a function of NO_x and NH_3 emissions. Simulation results have indeed often been presented as 2D isopleths of PM2.5 or nitrate as a function of precursor emissions, which allows showing in a comprehensive manner their sensitivity, and also, in a qualitative manner, non-linear effects (for example Watson et al., 1994 over USA; Xing et al., 2018 over the Beijing–Tianjin–Hebei region in China). Figure 6 shows the PM2.5 isopleths obtained through an interpolation among the 25 simulation concentration values (these 25 simulations correspond to the white square symbols in each isopleth diagram) at the three locations Be, Ma, and Bo previously defined. The X and Y-axes represent the strengths of the NH_3 and NO_x

Atmospheric
Chemistry
and Physics
Discussions

emission sources, respectively. With this type of graphical representation, it is possible to visualize the response of PM2.5 to a NO_x emission change by moving vertically, the reaction to a NH_3 emission change by moving horizontally or the reaction to a combined NO_x-NH_3 emission change by moving diagonally. The larger the number
260 of isopleths we cross on the path (high gradient), the larger the expected impact from an emission reduction will be. A simple theoretical model to generate and interpret these isopleths is proposed in Annex 2.

From the analysis of the isopleths, we note the following points:

- The diagram areas can be divided into two zones separated by a ridge (dashed line in Figure 6). Above the ridge line, PM2.5 is more sensitive to NH_3 while below the ridge line, it is more sensitive to NO_x emission reductions.
265 The orientation of the ridge (tending to vertical or horizontal) informs on the type of chemical regime (NO_x or NH_3 sensitive, respectively).
- In general the isopleths show a regular pattern with a progressive decrease of PM2.5 concentration when either the NO_x or NH_3 emissions are reduced, with the only exception of Bergamo during wintertime, where NO_x reductions up to 70% lead to a small increase of PM2.5 (Figure 6 - top left), whatever the reduction in NH_3
270 emission is. We discuss this particular feature later in this section.
- The efficiency of a NO_x vs NH_3 emission reduction varies across locations. We can compare the efficiency of a given reduction by looking at the horizontal (for NO_x) and vertical (for NH_3) gradients. To support this comparison, we included in each diagram dashed oblique lines that connect similar PM2.5 concentration values for single NO_x and NH_3 emission reductions. The more vertical are these lines, the larger is the NH_3 abatement
275 impact compared to the NO_x abatement impact. Conversely, the more horizontal they are, the larger is the NO_x abatement impact compared to the NH_3 abatement impact. For moderate emission reductions (up to 50%, top right corner), different behaviours are observed: while in Bergamo PM2.5 is more sensitive to NH_3 reductions, it is more sensitive to NO_x reductions in Mantova, and equally sensitive to both precursors in Bologna. This corresponds to the spatial patterns of NO_x- and NH_3-senstivive regimes depicted in Fig. 3.
280 - Winter- and summertime isopleths show completely different patterns in Bergamo whereas at the two other locations, they remain similar.
- At Mantova where moderate NO_x reductions (e.g. 50%) are the most efficient among the 3 sites, NH_3 emission reductions are more efficient than NO_x emission reductions for larger additional reductions (going for example from 75% to 100%). At Bergamo, NH_3 reductions are the most effective for moderate reductions whereas NO_x
285 reductions become more effective for larger reductions, as seen by the isopleths spacing. This confirms the findings of reversed chemical regimes for larger additional emission reductions detailed in the previous section.

The special pattern of Bergamo's PM2.5 isopleths during wintertime needs some additional discussion. The increase of the inorganic fraction of PM2.5 as a response to NO_x reductions during wintertime has already been noted by several authors (e.g. Le et al., 2020; Sheng et al., 2018). It has been related to an increase in the oxidizing capacity
290 of the atmosphere and in particular to increased ozone levels. This is due to the prevailing titration of O_3 by NO in wintertime high NO_x conditions and in the absence of photochemical ozone production due to reduced solar radiation (Kleinman et al., 1991).

$$NO(g) + O_3(g) \rightarrow NO_2(g) + O_2(g) \qquad (8)$$
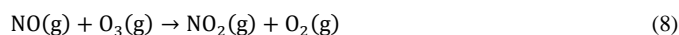
Accordingly, for a factor of two NO_x emissions decrease, Figure 8 shows roughly a factor of two increase for ozone,
295 while NO_2 decreases by a factor of less than two (1.7). These compensating changes result in a small increase in NO_3 radical production, the initial step of the major pathway of wintertime HNO_3 and nitrate formation (Kenagy et al., 2018).
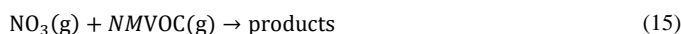
$$NO_2(g) + O_3(g) \rightarrow NO_3(g) \qquad (9)$$

In this pathway, the NO_3 radical formation is followed by combination with NO_2 to form N_2O_5, a reversible process,
300 and heterogeneous HNO_3 formation on wet particle surfaces.

$$NO_3(g) + NO_2(g) \leftrightarrow N_2O_5(g) \qquad (10)$$

$$N_2O_5(g) + H_2O(\text{aerosol surface}) \rightarrow 2HNO_3(g) \qquad (11)$$

The NO_3 radical has three major rapid sinks, reaction with NO, photolysis, and reaction with NMVOC's especially terpenes.

$$NO_3(g) + NO(g) \rightarrow 2NO_2(g) \qquad (12)$$

$$NO_3(g) + h\nu \rightarrow NO_2(g) + O(g) \qquad (13)$$

$$NO_3(g) + h\nu \rightarrow NO_2(g) + O_2(g) \qquad (14)$$

$$NO_3(g) + NMVOC(g) \rightarrow \text{products} \qquad (15)$$

Reactions 8 to 15 induce additional dependence of HNO_3 formation on NO_x species on top of (5), but which partly cancel out, as they are both involved in formation and sink processes.

SOA is formed through a series of chemical reactions of gaseous precursors (mainly volatile , intermediate volatile or semi-volatile organic compounds [VOCs] with the oxidants O_3, OH and nitrate radical (NO_3) (Li et al., 2011).

$$(S, I)VOC(g) + \text{oxidants} \rightarrow (S, I)OVOC(g) \leftrightarrow SOA(s) \qquad (16)$$
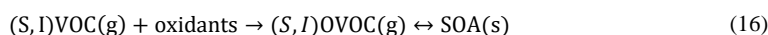
Putting all the arguments together, it follows that wintertime ammonium nitrate formation over Bergamo is most probably controlled by NO_3 radical formation (9), and its strong non-linearity with respect to NO_x emissions. The fact that this behaviour is observed in Bergamo and not in Mantova or Bologna is due to the much larger NO_2 levels in the Bergamo - Milano area (above 50 µg/m^3 during winter, Fig.2). Such large NO_2 levels are also simulated locally over the Turin area, and also lead to a slightly NH_3 sensitive regime there despite a G-ratio well above unity. Beyond 50% NO_x reduction, NH_4NO_3 formation decreases because NO_2 decreases more rapidly than ozone increases up to its maximum (at 75% NO_x emission reduction, see Figure 7).

This non-linearity between NO_x emission reductions and HNO_3 formation also explains the apparent discrepancies with the analysis of G-ratio indicating stronger sensitivity to HNO_3. Simply, sensitivity to HNO_3 concentration cannot be extrapolated to sensitivity to NO_x emissions in case of the above shown non-linear behaviour. Total nitrate is less abundant, but NO_x emission reductions below about 50% do not reduce it, and NH_3 emission reductions are thus more efficient, even if NH_3 is more abundant than HNO_3. In this respect, the complementary analysis of emission sensitivity and G-ratio gives interesting clues on possible non- linearity in the NO_x – HNO_3 relationship.

At Bergamo during winter, the increase in PM2.5 (+ 1.8 µg/m³) arising from a 50% reduction in NO_x emission also results from an increase in sulfate (+ 0.3 g/m³) and in SOA (+ 0.6 g/m³) concentrations. Both sulfate and SOA concentrations are closely related to O_3 concentrations (Figure 7). The sulfate increase is comparable in magnitude to the nitrate increase, even if sulfate levels are much smaller that nitrate ones. Figure 8 actually shows a strikingly similar response of sulfate, SOA and ozone to NO_x emission reductions (given that SO_2 and NMVOC emissions are held constant). Indeed the prevailing wintertime aqueous production of H_2SO_4 requires oxidants and in particular ozone (Le et al., 2020; Sheng et al., 2018). In addition, the formation of SOA in both the gas and particulate phases also requires oxidants (Vahedpour et al., 2011; Huang et al., 2020; Feng et al., 2016; Li et al., 2011; Tsimpidi et al., 2010).

Pinder et al. (2008) also note an oxidant limitation for SIA formation over Eastern United states for the 2000 to 2020 period, but in their simulations, it mainly affects sulfate that increases as a result of NO_x emission reductions while

nitrate decreases. This is due to a more important sulfate to nitrate ratio in eastern US than over the Po basin. Fu et al. (2020) derive from combined measurements and modelling that wintertime nitrate during haze events in the North China Plain (NCP) are nearly insensitive to 30% NO_x emission reductions, because increased ozone levels increase the NO_x to HNO_3 conversion efficiency. Following these authors, this conversion also involves the homogeneous HNO_3 formation via the $NO_2 + OH$. This reaction also could play a role in the Po basin, in addition to the heterogeneous pathway. Also Leung et al. (2020) simulate that wintertime nitrate abatement in the NCP is buffered with respect to emission reductions by increased oxidant build-up, but also by sulfate to nitrate conversion by liberating free NH_3 through sulfate concentration reduction, which can then enhance nitrate formation. Womack et al. (2019) find an oxidant limitation of nitrate formation over wintertime Utah (USA), and show that nitrate concentration diminishes when reducing VOC emissions.

5. Analysis of non-linearities

Clappier et al. (2020) highlighted the specificities of the Po basin area within Europe. They showed that non-linearities are important in this region. One peculiarity of the Po basin is a marked difference between the chemical regimes encountered within a confined area, that have implications on the linearity of PM2.5 responses to emission changes. In this section, we analyse in more details these non-linearities.

Information on the interaction term at reduction level α=25%: $\hat{P}_{NO_xNH_3}^{25\%}$ [$= P_{NO_xNH_3}^{25\%} - (P_{NO_x}^{25\%} + P_{NH_3}^{25\%})$] (first non-linear term in Eq. 4) is provided both spatially and as a scatter plot in Figure 8. This interaction term is almost constant (~0.9) over the entire domain, regardless of the chemical regimes (Figure 3) and regardless of the season (only the yearly average is shown in Figure 9, but the maps for both seasons are almost identical). At α=25%, the interaction terms therefore represents approximately 10% of the overall concentration change ($P_{NO_xNH_3}^{25\%}$). Single impacts would therefore lead to an overestimation (of about 10%) in PM2.5 reduction if added to extrapolate linearly the impact on yearly averaged PM2.5 concentrations of a combined NO_x-NH_3 emission reduction at 25%. Qualitatively, this behaviour is explained by the PM2.5 isopleths determined for 3 different sites of the domain (Figure 6). Their hyperbolic shapes indicate this negative non-linearity in the NH_3-NO_x interaction. As discussed in Annex 2, linearity would result in isopleths parallel to the descending diagonal lines.

When emission reductions increase from 25% to 50%, three additional non-linear terms are generated (three last terms in equation 4). Figure 9 and 10 provide an overview of these non-linear terms during wintertime and summer time, respectively. The top left panel of each figure represents their sum, i.e. the total nonlinearity generated between 25 and 50%. The right column shows the non-linearities associated to NO_x and NH_3 while the bottom left panel reports the non-linear interaction between the two precursors.

Overall, non-linearities are more important during wintertime than during summertime. This is true both in absolute and relative (not shown) terms. Non-linearities tend to be the largest in between areas that are characterised by well-marked NH_3- or NO_x-sensitive regimes (indicated by the blue and red drawn contours). This can be explained by the fact that when one of the two components (NO_x or NH_3) is in large excess (compared to the other one), reductions of this compound have then only little impact, implying that both single and combined reductions only involve one compound and are therefore similar.

During wintertime, the overall non-linearity (Figure 9 top left) is dominated by the single NO_x-related non-linearity ($\hat{P}_{NO_x}^{50-25\%}$, Figure 9 top right), a singularity in Europe as the Po basin is the only area where this occurs to this extent (Clappier et al., 2020). In the region of Bergamo, the NO_x non-linearity remains relatively weak despite the peculiar PM2.5 responses to NO_x emission reductions (i.e. an increase of PM2.5 concentrations for NOx emission reduction up to 50%, Figure 7). In this NH_3 sensitive region, this behaviour can be explained by the strong oxidant limitation of HNO_3 formation outlined above (Figure 8). It is worth mentioning that although atypical, this behaviour is quasi-linear with responses that remain proportional to the emission reduction strength but with a negative slope. Finally, the non-linear interactions (Figure 9, bottom left) are mostly negative, i.e. the sum of impacts resulting from single reductions exceeds the impact of the combined reduction as already observed for the 25% emission reductions.

385 In relative terms, the overall wintertime non-linearity terms increase by about 30 % when emission reductions increase from 25 and 50% (Figure 11 top, blue points). Note that these non-linearity terms reach larger values in some places of the modelling domain as highlighted by the data point dispersion.

During summer time, non-linear terms are smaller. The overall non-linearity term (Figure 10 top left) is dominated by the NH_3-NO_x non-linear interaction term ($\hat{P}_{NO_xNH_3}^{50-25\%}$, Figure 10 bottom left). In summer, PM2.5 concentration is NO_x sensitive in almost all the domain (Figure 3) and emission reductions do not lead to shifts in the chemical regimes. In this case, the interaction terms become more important. The largest non-linear interaction terms appear

390 in the western and northern part of the Po basin. They are everywhere negative, implying again that the sum of the impacts resulting from single reductions exceeds the impact of the combined reduction.

In relative terms, the mean overall summer time non-linearity term increases by about 10 % when emission reductions increase from 25 and 50% (Figure 11 top, red data points). In contrast to wintertime, non-linearities are approximately constant throughout the domain as highlighted by the very low Root Mean Square (RMS) errors.

395 Figure 11 shows the increases of the overall non-linear terms for emission reduction increasing from 25 to 50%, from 50 to 75%, and finally from 75 to 100%. Regardless of the emission reduction increments, summer time non-linearities remain small all over the domain with regression slope close to 0.9 and very limited data point dispersions (i.e. low RMSE). Wintertime non-linearities further increase significantly from 50% to 75% reduction levels (regression fit parameter close to 1.21) but tend to stabilize between 75 and 100% reduction level (regression fit

400 parameter close to 1.05). It is interesting to note that potentials in winter increase for all segments (all winter points are above the 1:1 line) indicating that the same percentage reduction (25%) gains progressively more impact when more intense reductions are considered.

6. Discussion

When designing air quality plans, it is important to identify the key precursors on which to act in priority to hit a

405 specific air quality target, but also to understand the consequences of these choices for various seasons (temporal variations), locations (spatial variability), emission reduction levels (strength) and strategies (combined or single emission reductions). As the information to make this decision is generally incomplete, assessing the robustness of the available model responses is essential. From the results presented here, a few key points appear.

410 • The seasonal and spatial variabilities in the response of PM2.5 to the reduction of NO_x and NH_3 emissions are extremely large, with different and sometimes opposite responses to emission changes. Yearly averages do not represent the appropriate time window to evaluate the impact of such emission reductions and a focus on wintertime (November to February) seems to be the right option, especially because concentrations are larger during this period of the year.

415 • The responses of PM2.5 to emission reduction plans that cover the whole area (i.e. uniform emission reductions are applied everywhere in the domain) vary from location to location: opposite responses occur within a few hundreds of kilometres for some reduction levels. In the region of Bergamo, PM2.5 response to NOx emission reductions can be negative, meaning an increase of PM2.5 when reducing the NO_x emissions. It is important to combine NO_x and NH_3 emission reductions in winter, or to go for stronger

420 emission reductions to make sure these unwanted effects are limited.

• Despite quite important non-linearities, PM2.5 responses to emission reductions are not chaotic. Indeed, regardless of the emission reduction level, the non-linear terms related to NH_3 emission reduction and to NO_x-NH_3 interactions are quite uniform spatially. This is not the case of NO_x emission reduction, for

425 which care must be taken to ensure that the detailed response of PM2.5 is captured.

• Although they are location dependent, PM2.5 isopleths represent an interesting tool to assess the impact of different NO_x and NH_3 emission reductions on PM2.5 concentration. They indeed allow visualising in one single diagram the impact of any type of reductions on concentrations in a single grid cell (or set of grid

430 cells).

Atmospheric
Chemistry
and Physics
Discussions

7. Conclusions

In this work, we analysed the sensitivities of PM2.5 to NO_x and NH_3 emissions by means of a set of EMEP simulations performed with different levels of emission reductions, from 25% up to a total switch-off of those emissions. Both single and combined precursor reduction scenarios were applied to determine the most efficient emission reduction strategies and quantify the interactions between NO_x and NH_3 emission reductions. The results confirmed the peculiarity of secondary inorganic PM2.5 formation in the Po basin suggested by Clappier et al. (2020), characterised by contrasting chemical regimes within distances of few (hundreds of) kilometres, as well as strong non-linear responses to emission reductions during wintertime. One of the striking results is the increase of the PM2.5 concentration levels when NO_x emission reductions are applied in NO_x-rich areas, such as the surroundings of Bergamo. The isopleths in the graphs showing PM2.5, nitrate, sulfate, SOA and O_3 concentrations as a function of NH_3 and NO_x emissions (Figure 7) indicate that the increased oxidative capacity of the atmosphere is the cause of the increase of PM2.5 induced by a reduction in NO_x emission up to -50%. This process can have contributed to the absence of significant PM2.5 concentration decrease during the COVID-19 lockdowns in many European cities (EEA, 2020; Putaud et al., 2020). It is important to account for this process when designing air quality plans, since it could well lead to transitionary increases in PM2.5 at some locations in winter as NO_x emission reduction measures are gradually implemented. At this type of location, mitigation measures that would be optimal in the long-term might not be efficient in the short-term.

Joint analysis of the G-ratio and emissions sensitivities can give a clue if a NH_3 sensitive chemical regime is due to either a limitation of NH_3 or to a lack of sensitivity of NOx emission reduction, due to a non-linear and opposite behaviour of the NO_x – HNO_3 relationship. In this latter case, the chemical regime is NH_3 sensitive in terms of NH_3 and NOx emission reductions, but HNO_3 limited in terms of G-ratio, as observed for the Bergamo – Milano region. Inversely, a positive G-ratio indicating HNO_3 limitation does not necessarily indicate a larger sensitivity to NOx than to NH_3 emissions. Thus, the results indicate the impossibility to directly use the G-ratio for air quality management, an interesting result in itself. Whereas PM2.5 responses expressed as potentials (i.e. responses projected linearly to a 100% emission reductions) of NO_x and NH_3 emission reduction show large variations seasonally and spatially, they are quite insensitive to the emission reduction levels at least up to -50% because the secondary aerosol formation chemical regimes are not modified by those relatively moderate ranges. The response of PM2.5 concentrations to emission reductions is found to be non-linear in certain areas of the Po basin, especially in winter. However, non-linear terms remain quite constant spatially (although they depend on the emission reduction strength), which suggests that potential approaches to model or parameterize these non-linearities might not be too complex to develop. These parametrisations might be useful to interpolate existing modelling responses to situations that are not explicitly modelled, or for their implementation in source – receptor models.

Since sulfate concentrations are low in the Po basin, the impact of SO_2 emission reductions was not evaluated here. However, the simulations performed in Clappier et al. (2020) indicate that air quality improvement plans addressing SO_2 emissions may still lead to additional PM2.5 decreases. Further works should also test if NMVOC emission would further affect the concentration of oxidants, and subsequently of nitrate (and sulfate) during winter. This depends on the fraction of ozone formed photochemically in the Po basin, compared to the one transported from outside by advection or entrainment.

Finally, it would be important to compare the results obtained in this work from the EMEPrv4_17 model with similar results obtained from other models. With its complex setting, the Po basin represents a good test case for such inter-comparisons.

References

Ansari, A.S., Pandis, S., 1998. Response of inorganic PM to precursor concentrations. Environ. Sci. Technol. 32, 2706–2714.

Beekmann, M., Prévôt, A. S. H., Drewnick, F., Sciare, J., Pandis, S. N., Denier van der Gon, H. A. C., Crippa, M., Freutel, F., Poulain, L., Ghersi, V., Rodriguez, E., Beirle, S., Zotter, P., von der Weiden-Reinmüller, S.-L., Bressi, M., Fountoukis, C., Petetin, H., Szidat, S., Schneider, J., Rosso, A., El Haddad, I., Megaritis, A., Zhang, Q. J., Michoud, V., Slowik, J. G., Moukhtar, S., Kolmonen, P., Stohl, A., Eckhardt, S., Borbon, A., Gros, V., Marchand,

Atmospheric
Chemistry
and Physics
Discussions

480   N., Jaffrezo, J. L., Schwarzenboeck, A., Colomb, A., Wiedensohler, A., Borrmann, S., Lawrence, M., Baklanov, A.,
       and Baltensperger, U.: In situ, satellite measurement and model evidence on the dominant regional contribution to
       fine particulate matter levels in the Paris megacity, Atmos. Chem. Phys., 15, 9577–9591,
       https://doi.org/10.5194/acp-15-9577-2015, 2015.

       Bessagnet, B., Beauchamp, M., Guerreiro, C. et al. (2014). Can further mitigation of ammonia emissions reduce
485   exceedances of particulate matter air quality standards? Environmental Science & Policy, 44, 149–163.
       DOI:10.1016/j.envsci.2014.07.011

       Blanchard, C.L.; Hidy, G.M. Effects of Changes in Sulfate, Ammonia,and Nitric Acid on Particulate Nitrate
       Concentrations in the South-eastern United States;J. Air & Waste Manage. Assoc.2003,53, 283-290.

       Carnevale C., E. Pisoni, M Volta, 2020. A non-linear analysis to detect the origin of PM10 concentrations in
490   Northern Italy, Science of the Total Environment 409 (2010) 182–191

       Clappier, A., P., Thunis, J.P., Putaud, M., Beekmann, A. Demeij, 2021: Analysis of the chemical regimes and non-
       linearity associated to PM2.5 in Europe. Submitted in Environment International.

       De Meij A., M. Krol, F. Dentener, E. Vignati, C. Cuvelier, The sensitivity of aerosol in Europe to two different
       emission inventories and temporal distribution of emissions, Atmos. Chem. Phys., 6, 4287–4309, 2006.

495   De Meij A., P. Thunis, B. Bessagnet, C. Cuvelier, The sensitivity of the CHIMERE model to emissions reduction
       scenarios on air quality in Northern Italy., Atmos. Env. Volume 43, Issue 11, Pages 1897-1907, April 2009.

       Dodge, M. C.: Effect of selected parameters on predictions of a photochemical model, US Environmental Protection
       Agency, EPA-600/3-77/048, Research Triangle Park, NC, USA, 1977.

       EDGAR2020, Emission Database for Global Atmospheric research, https://edgar.jrc.ec.europa.eu/

500   EEA2020, Air quality in Europe — 2020 report, EEA Report No 11/2020

       EMEP 2003, Transboundary acidification and eutrophication and ground level ozone in Europe: Unified EMEP
       model description" EMEP/MSC-W Report 1/2003.
       https://emep.int/publ/reports/2003/emep_report_1_part1_2003.pdf

       EMEP 2011, EMEP/MSC-W Model - User s Guide July 2011.
505   https://wiki.met.no/_media/emep/page1/userguide_062011.pdf

       Fagerli et al., 2004 H. Fagerli, D. Simpson and S. Tsyro. Unified EMEP model: Updates. In EMEP Status Report
       1/2004, Transboundary acidification, eutrophication and ground level ozone in Europe. Status Report 1/2004, pages
       11–18. The Norwegian Meteorological Institute, Oslo, Norway, 2004.

       Feng, T., Li, G., Cao, J., Bei, N., Shen, Z., Zhou, W., Liu, S., Zhang, T., Wang, Y., Huang, R.-J., Tie, X. and
510   Molina, L. T., 2016: Simulations of organic aerosol concentrations during springtime in the Guanzhong Basin,
       China, Atmos. Chem. Phys., 16(15), 10045–10061, doi:10.5194/acp-16-10045-2016.

       Feng, T., Zhao, S., Bei, N., Wu, J., Liu, S., Li, X., Liu, L., Qian, Y., Yang, Q., Wang, Y., Zhou, W., Cao, J., and Li,
       G.: Secondary organic aerosol enhanced by increasing atmospheric oxidizing capacity in Beijing–Tianjin–Hebei
       (BTH), China, Atmos. Chem. Phys., 19, 7429–7443, https://doi.org/10.5194/acp-19-7429-2019, 2019.

515   Fu, X., Wang, S., Xing, J., Zhang, X., Wang, T., and Hao, J.: Increasing Ammonia Concentrations Reduce the
       Effectiveness of Particle Pollution Control Achieved via SO2 and NOX Emissions Reduction in East China,
       Environ. Sci. Tech. Let., 4, 221–227, https://doi.org/10.1021/acs.estlett.7b00143, 2017.

       Fu X, Wang T, Gao J, Wang P, Liu Y, Wang S, Zhao B, Xue L. Persistent Heavy Winter Nitrate Pollution Driven
       by Increased Photochemical Oxidants in Northern China. Environ Sci Technol. 2020 Apr 7;54(7):3881-3889. doi:
520   10.1021/acs.est.9b07248. Epub 2020 Mar 16. PMID: 32126767.

Hakimzadeh M., E. Soleimanian, A. Mousavi, A. Borgini, C. De Marco, A. Ruprecht, C. Sioutas, 2020. The impact of biomass burning on the oxidative potential of PM2.5 in the metropolitan area of Milan, Atmospheric Environment 224 (2020) 117328

525   Huang L., Q. Wanga, Y. Wang, C. Emeryc, A. Zhua, Y. Zhua, S. Yina, G. Yarwood, K. Zhang, L. Li, 2020: Simulation of secondary organic aerosol over the Yangtze River Delta region: The impacts from the emissions of intermediate volatility organic compounds and the SOA modeling framework, Atmospheric Environment, https://doi.org/10.1016/j.atmosenv.2020.118079.

Kenagy, H. S., Sparks, T. L., Ebben, C. J., Wooldrige, P. J., Lopez-Hilfiker, F. D., Lee, B. H., et al. (2018). NOx lifetime and NOy partitioning during WINTER. Journal of Geophysical Research: Atmospheres, 123, 9813–9827.
530   https://doi.org/10.1029/2018JD028736

Kleinman L.I., Seasonal dependence of boundary layer peroxide concentration: The low and high NOx regimes, J. Geophys. Res, vol.96, pp.20721-20733, 1991.

Kroll, J.H., J. H. Seinfeld, 2008: Chemistry of secondary organic aerosol: Formation and evolution of low-volatility organics in the atmosphere, Atmospheric Environment 42 (2008) 3593–3624.

535   Lachatre, M., Fortems-Cheiney, A., Foret, G., Siour, G., Dufour, G., Clarisse, L., Clerbaux, C., Coheur, P.-F., Van Damme, M., and Beekmann, M.: The unintended consequence of SO2 and NO2 regulations over China: increase of ammonia levels and impact on PM2.5 concentrations, Atmos. Chem. Phys., 19, 6701–6716, https://doi.org/10.5194/acp-19-6701-2019, 2019

Larsen, B., Gilardoni, S., Stenström, K., Niedzialek, J., Jimenez, J., and Belis, C.: Sources for PM air pollution in
540   the Po Plain, Italy: II. Probabilistic uncertainty characterization and sensitivity analysis of secondary and primary sources, Atmos. Environ., 50, 203–213, https://doi.org/10.1016/j.atmosenv.2011.12.038, 2012.

Le T., Wang Y., Liu L., Yang J., Yung Y., Li G., and Seinfeld J., 2020: Unexpected air pollution with marked emission reductions during the COVID-19 outbreak in China, Science, 369, eabb7431,10.1126/science.abb7431, 2020.

545   Leung D., Hongrong Shi, Bin Zhao, Jing Wang, Elizabeth M. Ding, Yu Gu, Haotian Zheng, Gang Chen, Kuo-Nan Liou, Shuxiao Wang, Jerome D. Fast, Guangjie Zheng, Jingkun Jiang, Xiaoxiao Li, Jonathan H. Jiang : Wintertime Particulate Matter Decrease Buffered by Unfavorable Chemical Processes Despite Emissions Reductions in China, GRL, Volume47, Issue14, 2020, https://doi.org/10.1029/2020GL087721

Li, G., Zavala, M., Lei, W., Tsimpidi, A. P., Karydis, V. A., Pandis, S. N., Canagaratna, M. R., and Molina, L. T.,
550   2011: Simulations of organic aerosol concentrations in Mexico City using the WRF-CHEM model during the MCMA-2006/MILAGRO campaign, Atmos. Chem. Phys., 11, 3789-3809, https://doi.org/10.5194/acp-11-3789-2011.

Makar, P. A., Moran, M. D., Zheng, Q., Cousineau, S., Sassi, M., Duhamel, A., Besner, M., Davignon, D., Crevier, L.-P., and Bouchet, V. S.: Modelling the impacts of ammonia emissions reductions on North American air quality,
555   Atmos. Chem. Phys., 9, 7183–7212, https://doi.org/10.5194/acp-9-7183-2009, 2009.

Pay, M.T., Jimenez-Guerrero, P., Baldasano, J.M., 2012. Assessing sensitivity regimes of secondary inorganic aerosol formation in Europe with the CALIOPE-EU modeling system. Atmos. Environ. 51, 146–164.

Pernigotti, D.; Georgieva, E.; Thunis, P.; Bessagnet, B. Impact of meteorological modelling on air quality: Summer and winter episodes in the Po valley (Northern Italy). Int. J. Envir. Poll. 2014, 50, 111–119.

560   Petetin, H., Sciare, J., Bressi, M., Gros, V., Rosso, A., Sanchez, O., Sarda-Estève, R., Petit, J.-E., and Beekmann, M.: Assessing the ammonium nitrate formation regime in the Paris megacity and its representation in the CHIMERE model, Atmos. Chem. Phys., 16, 10419–10440, https://doi.org/10.5194/acp-16-10419-2016, 2016.

Pinder R. W., A. B. Gilliland and R. L. Dennis. Environmental impact of atmospheric NH3 emissions under present and future conditions in the eastern United States, Geophysical Research Letters, vol. 35, L12808, 2008

565 Putaud, J.P, Pozzoli, L., Pisoni, E., Martins Dos Santos, S., Lagler, F., Lanzani, G., Dal Santo, U., Colette, A., Impacts of the COVID-19 lockdown on air pollution at regional and urban background sites in northern Italy, ACPD, https://doi.org/10.5194/acp-2020-755,2020.

Raffaelli, K.; Deserti, M.; Stortini, M.; Amorati, R.; Vasconi, M.; Giovannini, G. Improving Air Quality in the Po Valley, Italy: Some Results by the LIFE-IP-PREPAIR Project. Atmosphere 2020, 11, 429

570 Ricciardelli I., D. Bacco, M. Rinaldi, G. Bonafe, F. Scotto, A. Trentini, G. Bertacci, P. Ugolini, C. Zigola, F. Rovere, C. Maccone, C. Pironi, V. Poluzzi, 2017. A three-year investigation of daily PM2.5 main chemical components in four sites: the routine measurement program of the Supersito Project (Po Valley, Italy), Atmospheric Environment 152 (2017) 418e430

Seinfeld, J. H. and Pandis, S.N: Atmospheric Chemistry and Physics: From Air Pollution to Global Change, 2nd
575 edn., J. Wiley and Sons, New York, 2006.

Shah V, Jaeglé L, Thornton JA, et al. Chemical feedbacks weaken the wintertime response of particulate sulfate and nitrate to emissions reductions over the eastern United States. Proceedings of the National Academy of Sciences of the United States of America. 2018 Aug;115(32):8110-8115. DOI: 10.1073/pnas.1803295115.

580 Sheng, Fang & Jingjing, Liu & Yu, Chen & Fu-Ming, Tao & Xuemei, Duan & Jing-yao, Liu. (2018). Theoretical study of the oxidation reactions of sulfurous acid/sulfite with ozone to produce sulfuric acid/sulfate with atmospheric implications. RSC Advances. 8. 7988-7996. 10.1039/C8RA00411K.

Shrivastava, M., et al. (2017), Recent advances in understanding secondary organic aerosol: Implications for
585 global climate forcing, Rev. Geophys., 55, 509–559, doi:10.1002/2016RG000540.

Simpson et al., 2003 D. Simpson, H. Fagerli, J.E. Jonson, S. Tsyro, P. Wind and J.-P. Tuovinen. The EMEP Unified Eulerian Model. Model Description. EMEP MSC-W Report 1/2003. The Norwegian Meteorological Institute, Oslo, Norway, 2003.
590

Simpson, D., Benedictow, A., Berge, H., Bergström, R., Emberson, L.D., Fagerli, H., Flechard, C.R., Hayman, G.D., Gauss, M., Jonson, J.E., Jenkin, M.W., Nyíri, Á, Richter, C., Semeena, V.S, Tsyro, S., Tuovinen, J.-P., Valdebenito, Á., and Wind, P.: The EMEP MSC-W chemical transport model – technical description.Atmospheric Chemistry and Physics, 12, 7825-7865, 2012. http://www.atmos-chem-phys.net/12/7825/2012/acp-12-7825-
595 2012.html

Stein, U. and P. Alpert, 1993: Factor separation in numerical simulations, J. Atmos. Sci., 50, 2107-2115.

Thunis P. and A. Clappier, 2014: Indicators to support the dynamic evaluation of air quality models,. Atmospheric Environment, 98, 402-409.

Thunis P., A. Clappier, E. Pisoni, B. Degraeuwe. Quantification of non-linearities as a function of time averaging in
600 regional air quality modeling applications, Atmospheric Environment, 103, 263-275, 2015.

Thunis P., D. Pernigotti, C. Cuvelier, E. Georgieva, A. Gsella, A. De Meij, G. Pirovanod, A. Balzarini, G. M. Riva, C. Carnevale, E. Pisoni, M. Volta, B. Bessagnet, A. Kerschbaumer, P.Viaene, K. De Ridder, A. Nyiri and P. Wind, POMI: A Model Intercomparison exercise over the Po valley, Air Quality, Atmosphere and health, DOI: 10.1007/s11869-013-0211-1, October 2013.

605 Tsimpidi, A. P., Karydis, V. A., Zavala, M., Lei, W., Molina, L., Ulbrich, I. M., Jimenez, J. L., and Pandis, S. N. 2010: Evaluation of the volatility basis-set approach for the simulation of organic aerosol formation in the Mexico City metropolitan area, Atmos. Chem. Phys., 10, 525–546, https://doi.org/10.5194/acp-10-525-2010.

Atmospheric
Chemistry
and Physics
Discussions

Tsigaridis, K., Daskalakis, N., Kanakidou, M., Adams, P.J., Artaxo, P., Bahadur, R., et al. The AeroCom evaluation and intercomparison of organic aerosol in global models. Atmos Chem Phys. 14(19), 10845–95.

610   doi.org/10.5194/acp-14-10845-2014.

Vahedpour M., M. Goodarzi , N. Hajari and F. Nazari , Struct. Chem., 2011, 22 , 817 —822

Watson J.G., Judith C. Chow , Fred W. Lurmann & Stefan P. Musarra (1994) Ammonium Nitrate, Nitric Acid, and Ammonia Equilibrium in Wintertime Phoenix, Arizona, Air & Waste, 44:4, 405-412, DOI: 10.1080/1073161X.1994.10467262

615

Womack, C. C., McDuffie, E. E., Edwards, P. M., Bares, R., de Gouw, J. A., Docherty, K. S., Dube, W. P., Fibiger, D. L., Franchin, A., Gilman, J. B., Goldberger, L., Lee, B. H., Lin, J. C., Long, R., Middlebrook, A. M., Millet, D. B., Moravek, A., Murphy, J. G., Quinn, P. K., Riedel, T. P., Roberts, J. M., Thornton, J. A., Valin, L. C., Veres, P. R., Whitehill, A. R., Wild, R. J., Warneke, C., Yuan, B., Baasandorj, M., and Brown, S. S.: An odd oxygen

620   framework for wintertime ammonium nitrate aerosol pollution in urban areas: NOx and VOC control as mitigation strategies, Geophys. Res. Lett., 46, 4971–4979, https://doi.org/10.1029/2019GL082028, 2019.

Xing, J., Ding, D., Wang, S., Zhao, B., Jang, C., Wu, W., Zhang, F., Zhu, Y., and Hao, J.: Quantification of the enhanced effectiveness of NOx control from simultaneous reductions of VOC and NH3 for reducing air pollution in

625   the Beijing–Tianjin–Hebei region, China, Atmos. Chem. Phys., 18, 7799–7814, https://doi.org/10.5194/acp-18-7799-2018, 2018.

Annex 1: Selection of seasons

630

Chemical regimes show a great variability with time. To select the extension of the seasons, we analyse the monthly behaviour of the NH_3 and NO_x responses as well as the interaction terms (Figure 12). The analysis is performed for two locations: Bergamo which lies in a NH_3 sensitive zone and Mantova which lies within a NO_x sensitive zone. On these plots, we identify two major seasons with a consistent behaviour: winter from November to February and
635 summer, from April to September. These two seasons are similar at both locations. The two remaining months, April and October are transition months and are not considered in the analysis. It is interesting to note that these two transition periods correspond more or less to the switching time between the NO_x and NH_3 concentration time profiles (Figure 12 - right panel). On the latter figures, the SO_2 and NO_2 temporal evolutions are almost identical, in contrast to NH_3.

Annex 2: A theoretical example for the isopleths

640

To facilitate the interpretation of the isopleths diagrams, we use a simple theoretical example that mimics the complex reactions process schematized by equations (5) and (6) above. Our simplified process is described by the following relation: $C_C(x, y) = \min(E_A[x], E_B[y])$ where C_c is the concentration of a compound "c" that is given by the minimum between two emitted species A and B. The concentration depends on the strengths of these emissions, specified by the parameters x and y. For each emission strength (x or y), the two emission species are proportional to
645 their full-scale value (100%): $E_A(x) = x E_A[100]$ and $E_B(y) = y E_B[100]$, respectively. If we choose $E_A(100) \gg E_B(100)$, we create a B-sensitive environment (Figure 13 - left column) and inversely (Figure 13 - right column). If we select mixed situations, representing for example an average of days, during which we alternate between A-sensitive and B-sensitive regimes, we obtain the two bottom isopleth diagrams that represent cases where a larger
650 number of A-sensitive (right) or B-sensitive (left) events are recorded. Although extremely simple, these diagrams illustrate properties that are observed on the real test cases.

Let's take the example of a A-sensitive regime. Similar observations can be made in the case of a B-sensitive regime. We note the following points:

- The diagram area can roughly be divided into two zones separated by a ridge: a top-left triangle where the
655 sensitivity to emission reductions of species "A" dominate and a bottom-right triangle where the sensitivity to B dominates. The slope of the ridge (larger or less than one) informs on the type of regime.
- In the case of a single A-sensitive day (top right) with $E_A(100)=2E_B(100)$, the concentration of compound C remains unchanged for emission reductions of A up to 50% while its concentration react in a linear way to emission changes of B from 0 to 100%. As concentration must drop to zero for full reductions of either A or B,
660 a lower gradient for B than A for small emission reductions implies a reversed behaviour (larger gradient for B than A) for larger reductions. In our simple example, the gradient of B is zero from 0 to 50% but is twice as large as A from 0 to 50% emission strength.
- While the combination of several events (e.g. days) characterised by different regimes leads to smoother isopleths (bottom), the same characteristics can be noted. In particular, the inclination (tending to the horizontal
665 or vertical) provides information on the type of chemical regime.
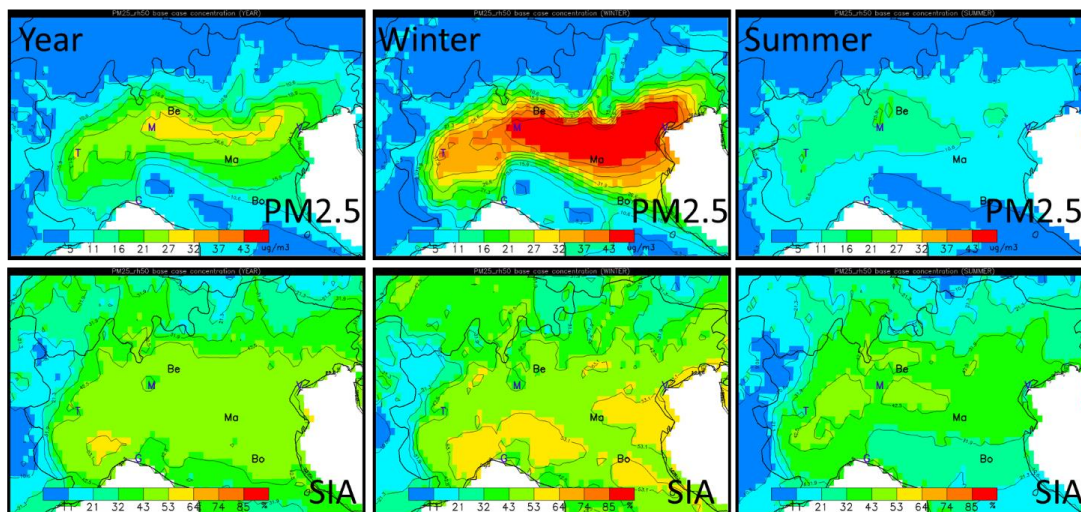
Figure 1: Seasonal variations of the base case PM2.5 (top row) and SIA (bottom row). The symbols: Be, Ma and Bo
670   **represent the locations selected for more detailed analysis: Bergamo (Be), Mantova (Ma) and Bologna (Bo). Other cities**
**are indicated by their first letter for convenience: Venice, Milan, Turin and Genova.**


Figure 2: Summer (top) and winter (bottom) concentration base-case fields for SO2 (left column), NO2 (central column)
675   **and NH3 (right column). The symbols: Be, Ma and Bo represent the locations selected for more detailed analysis:**
Bergamo (Be), Mantova (Ma) and Bologna (Bo). Other cities are indicated by their first letter for convenience: Venice,
Milan, Turin and Genova.
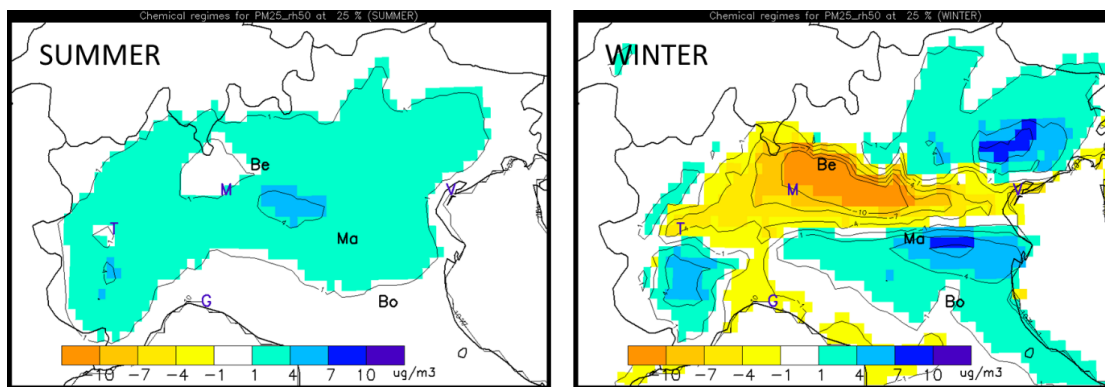
Figure 3: Winter (right) and Summer (left) chemical regimes obtained at a reduction level of α=25%. The maps represent the $P_{NO_x}^{25\%} - P_{NH_3}^{25\%}$ (unit: μg/m3) indicator that shows the NOx- and NH3-sensitive areas in blue and yellow, respectively. The symbols Be, Ma and Bo indicate the location of Bergamo, Mantova and Bologna, respectively. Other cities are indicated by their first letter for convenience: Venice, Milan, Turin and Genova.
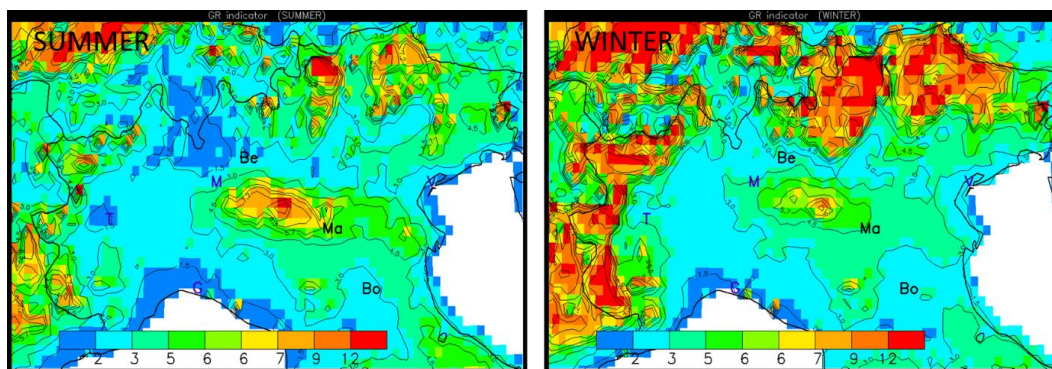

Figure 4: G-ratio for winter (right) and summer (left) times. The symbols Be, Ma and Bo indicate the location of Bergamo, Mantova and Bologna, respectively. Other cities are indicated by their first letter for convenience: Venice, Milan, Turin and Genova.
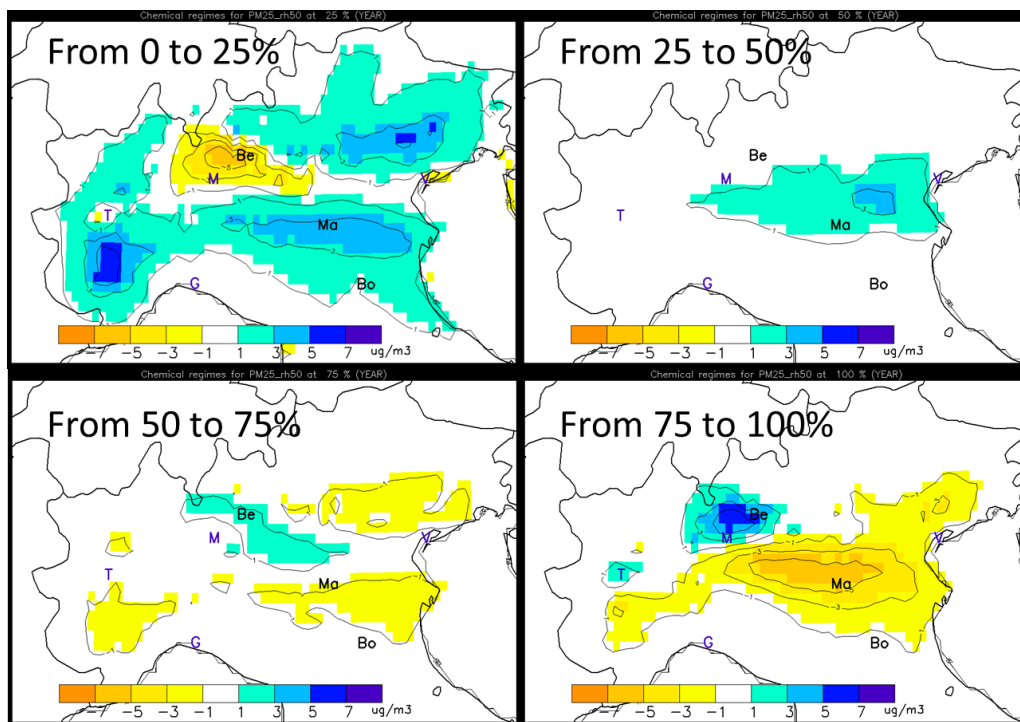
690 **Figure 5: Yearly averaged chemical regimes obtained for a 25% emission reduction starting at different levels of emissions corresponding to α=0, 25, 50 and 75. The maps represent the $(P_{NO_x} - P_{NH_3})$ between the starting and ending levels (unit: µg/m3) showing the NOx-and NH3 sensitive areas in blue and yellow, respectively. The symbols Be, Ma and Bo indicate the location of Bergamo, Mantova and Bologna, respectively. Other cities are indicated by their first letter for convenience: Venice, Milan, Turin and Genova.**

695
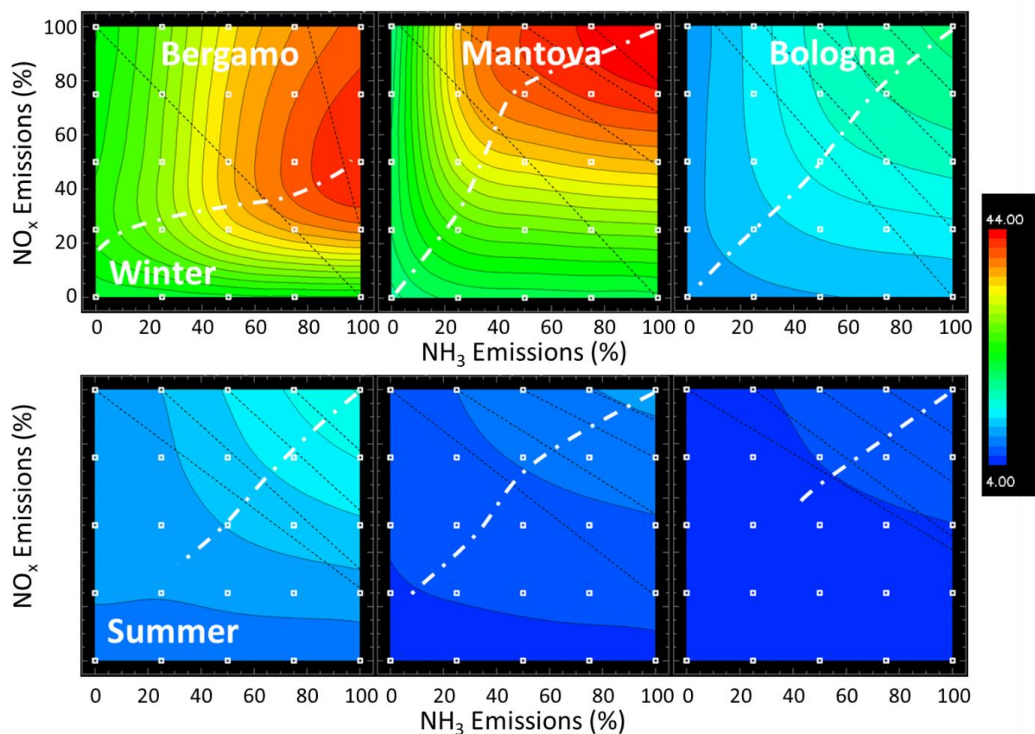
Figure 6: PM2.5 isopleths during Winter (top row) and Summer (bottom row) at the three locations of interest (see maps). PM2.5 concentrations are expressed in as a function of the intensity of the NOx (Y-axis) and NH3 (X-axis) emissions, respectively. The overlaid dashed oblique lines on each diagram connect similar PM2.5 concentration values for single NOx and NH3 reductions. The more vertical are these lines, the larger is the NH3 abatement impact compared to the NOx abatement impact; The more horizontal they are, the larger is the NOx abatement impact compared to the NH3 abatement impact. The dashed line delineates the ridge between the NH3 and NOx sensitive areas.

700
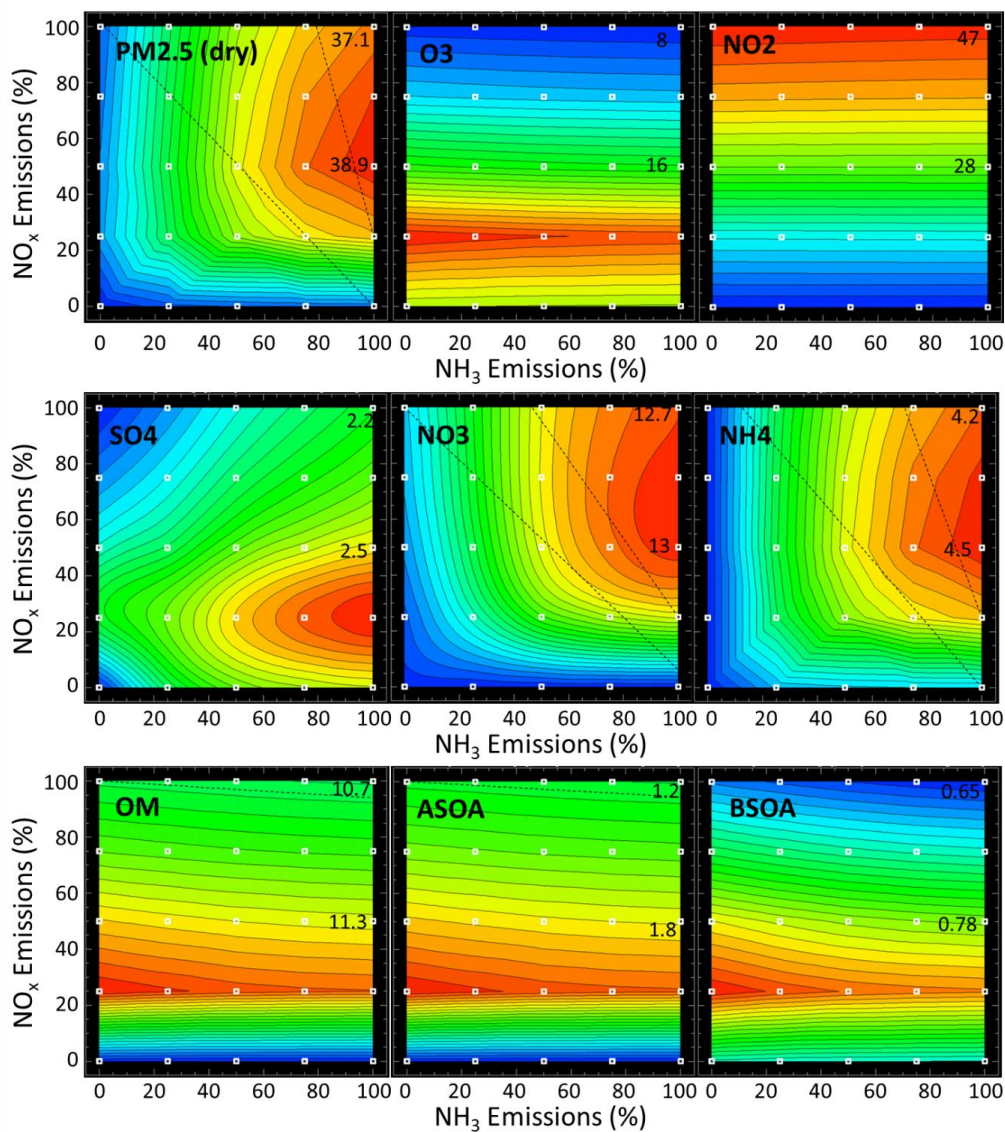
705 Figure 7: Wintertime isopleths in Bergamo for the species: dry PM2.5, O3, NO2, sulfate (SO4), nitrate (NO3), ammonium (NH4), organic matter (OM), anthropogenic and biogenic secondary aerosols (ASOA and BSOA, respectively). The two numbers on the vertical axis indicate concentration values for the base case and at the 50% NOx emission level.
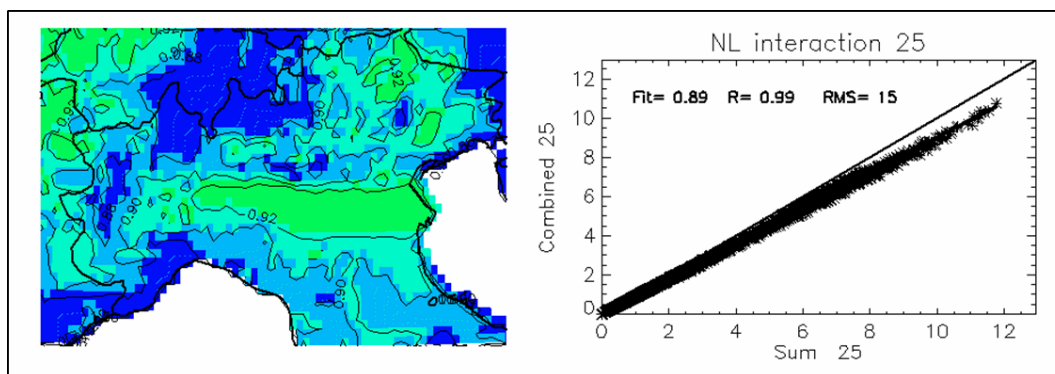
Figure 8: Yearly mean non-linear interaction term for a 25% reduction in NOx and NH3. The map (left) shows the ratio $\frac{P_{NO_xNH_3}^{25\%}}{P_{NO_x}^{25\%}+P_{NH_3}^{25\%}}$ whereas the scatter plot compares the sum of the impacts of the two-single reductions (X-axis) with the impact of the combined emission reduction (µg/m3) (Y-axis).
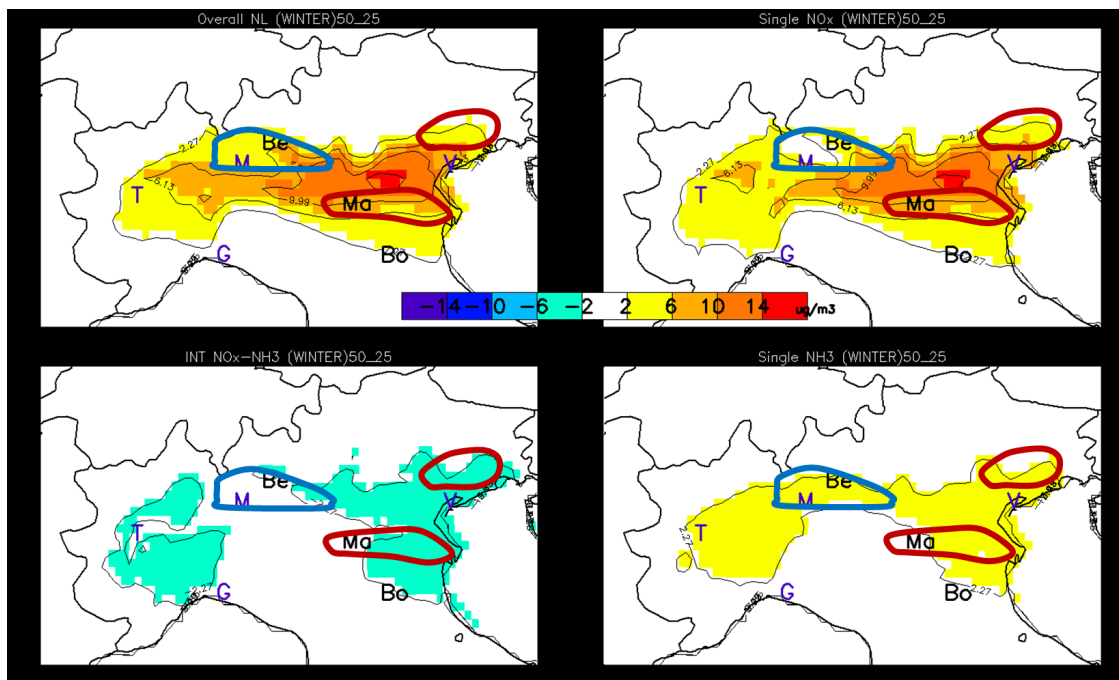
Figure 9: Wintertime maps of the overall non-linearity term (top left) and of its components: the single NOx non-linearity term (SNOx – top right), the single NH3 non-linearity term (SNH3 – bottom right) and the NOx-NH3 interaction term (INOXNH3 – bottom left). The three locations of interest: Bergamo, Mantova and Bologna are indicated by their first two letters while other cities are indicated with their first letter for convenience (Venice, Milan, Turin and Genova). The hand drawn contours roughly indicate the central position of the NH3 (blue) and NOx (red) sensitive regime areas (see Figure 3 - right).
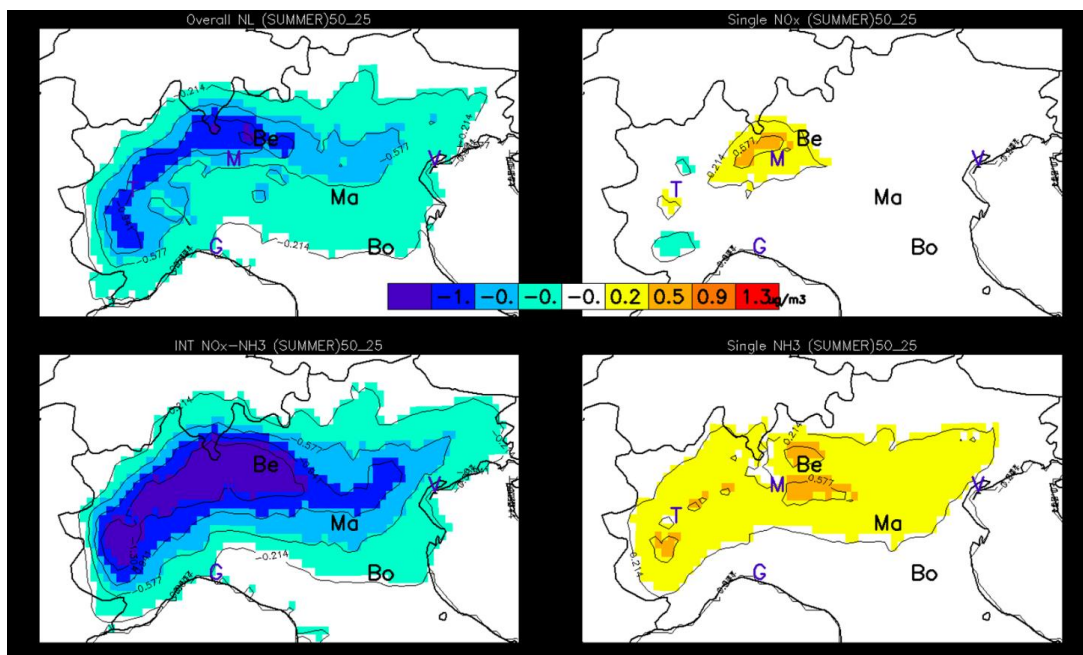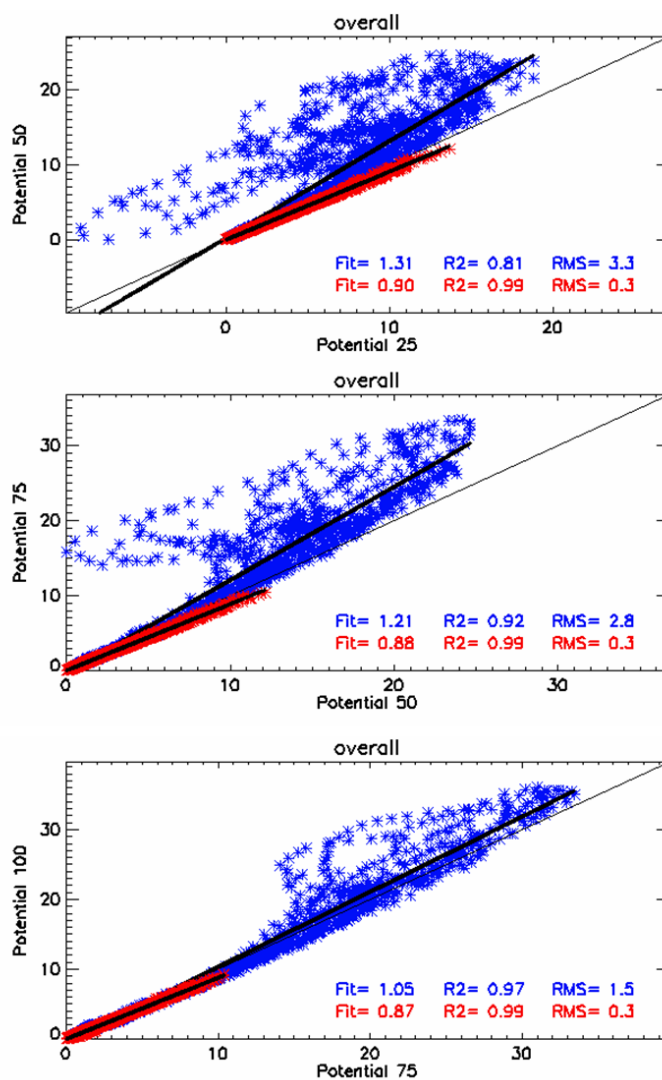
Figure 10: same as Figure 9 but for summer time.

Figure 11: Changes of the overall non-linearity terms from 25 to 50% (top), from 50 to 75% (middle) and from 75 to 100% (bottom) in NOx and NH3. Each point represents one land grid cell within the domain for wintertime (blue) and summer time (red). The "fit" parameter indicates the slope of the regression line while R2 and RMS provide information on the coefficient of determination and the root mean square error, respectively.

730

Figure 12: Monthly averaged responses to NH3 (blue), NOx (red) reductions (25%) and interaction terms (grey) at two locations: Bergamo (top) and Mantova (bottom). The right panel shows the monthly evolution of the concentrations of NO2, NH3 and SO2 at those two locations. Note that concentrations are normalised by their average values.
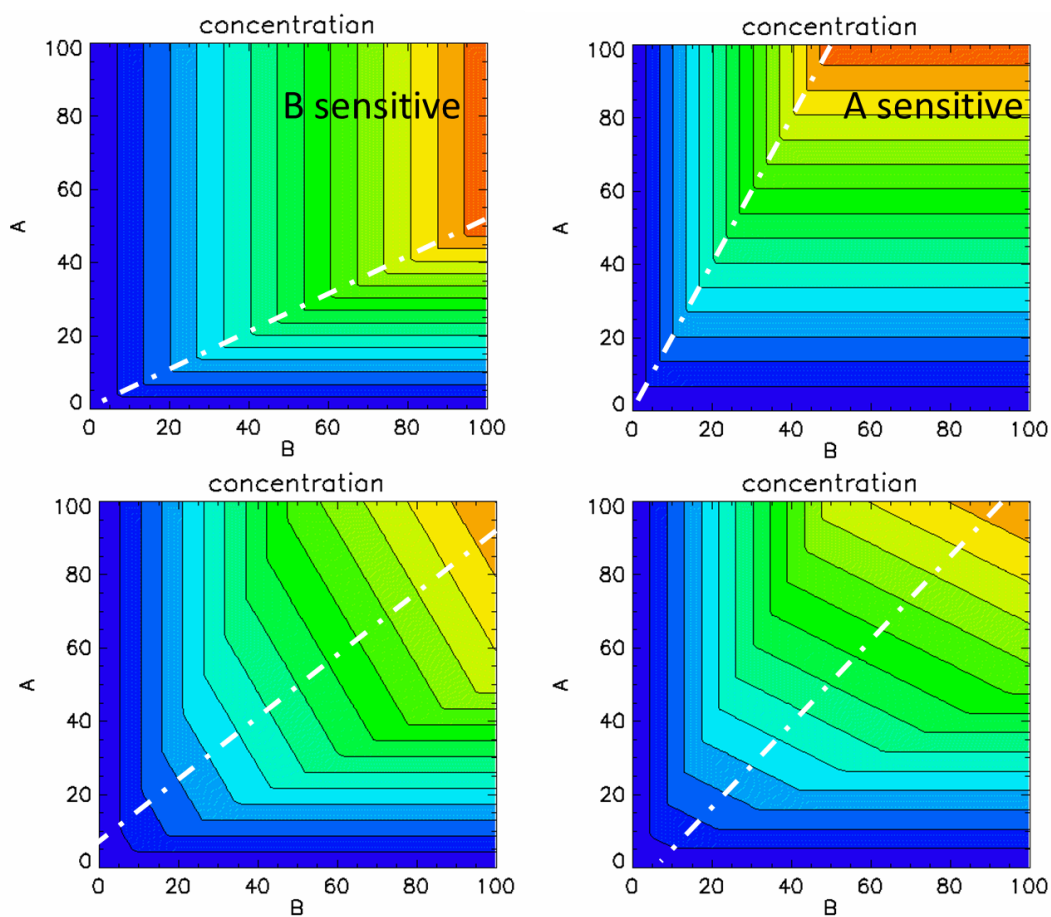
735   **Figure 13: Isopleths for a simple theoretical system consisting of two emission precursors (A and B) competing through non-linear reactions to the concentration of a pollutant. See details in the text.**

740